The Co-ordination Chemistry of Mixed Pyridine–Phenol Ligands; Spectroscopic and Redox Properties of Mononuclear Ruthenium Complexes with (Pyridine)$_{6-x}$(Phenolate)$_x$ Donor Sets (x = 1 or 2)†

Bridget M. Holligan, John C. Jeffery, M. Katharine Norgett, Erik Schatz and Michael D. Ward *
School of Chemistry, University of Bristol, Cantock's Close, Bristol BS8 1TS, UK

Two new ruthenium complexes containing N_5O and N_4O_2 donor sets (where N is a pyridyl donor and O a phenolate donor) were prepared, in order to study the electrochemical and spectroscopic consequences for the ruthenium centre of stepwise replacement of pyridyl ligands by phenolates. Reaction of the N,O bidentate ligand 2-(2-hydroxyphenyl)pyridine (HL^2) (for which a new synthesis is presented) with $[Ru(bipy)_2Cl_2]$ (bipy = 2,2'-bipyridine) in refluxing ethanol followed by treatment with KPF_6 gave $[Ru^{II}(bipy)_2L^2][PF_6]$ in near-quantitative yield. The crystal structure shows the expected pseudo-octahedral geometry, with the pyridyl ring *trans* to the phenolate exhibiting the shortest Ru–N distance [2.022(4) Å] due to enhanced $d_\pi(Ru)$–bipy(π^*) back bonding. The cyclic voltammogram shows that the presence of the phenolate ligand stabilises the ruthenium(III) state by +0.86 V relative to $[Ru(bipy)_3]^{2+}$; the UV/VIS spectrum is also assigned. Reaction of $RuCl_3$ with 2 equivalents of the N,N,O-terdentate ligand 6-(2-hydroxyphenyl)-2,2'-bipyridine (HL^1) in refluxing ethylene glycol followed by treatment with KPF_6 yielded $[Ru^{III}L^1_2][PF_6]$, which also has a pseudo-octahedral structure. The cyclic voltammogram shows that the presence of a second phenolate results in stabilisation of the ruthenium(III) state by a further +0.57 V, and also brings a usually inaccessible Ru^{III}–Ru^{IV} couple into the solvent window. Initial attempts to prepare $[RuL^2_3]$, with an N_3O_3 donor set, were unsuccessful.

In order to extend the chemistry of the well known polypyridine ligands[1,2] we have recently been interested in studying the co-ordination behaviour of polydentate ligands containing both pyridine and phenol groups as donors.[3–5] Three particular features of interest in these complexes have emerged from the initial studies with 6-(2-hydroxyphenyl)-2,2'-bipyridine (HL^1), an N,N,O-chelating analogue of 2,2':6',2''-terpyridine (terpy). First, the presence of a σ-donating phenolate group results in the ligand stabilising higher oxidation states than does terpy; this was observed in the cobalt(III) complex. Secondly, the presence of *bridging* phenolate ligands in some cases allows formation of magnetically coupled binuclear species in which parallel sections of adjacent ligands, lying between 3.3 and 4 Å apart, appear to be stabilised by π-stacking interactions. Thirdly, the ligands are considerably distorted from planarity, with torsion angles of up to 15° between the pyridyl rings and up to 40° between the central pyridyl and terminal phenol ligands. In the previous paper we examined the effects of ligand flexibility and π-stacking characteristics on complex structures, by comparing the crystal structures of the complexes of Cu^{II} and Ni^{II} with HL^1 and with 2-(2-hydroxyphenyl)-1,10-phenanthroline, which has the same donor set as HL^1 but is less flexible and more likely to display π-stacking interactions due to its extra aromatic ring.[5] In this paper we examine the electrochemical and spectroscopic consequences of the presence of phenolates in the ligand donor set, by examining mononuclear ruthenium complexes in which the donor set is varied from N_6 to N_4O_2 (where N is a pyridyl donor and O is a phenolate donor).

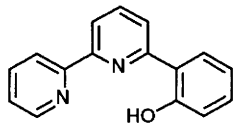

HL^1

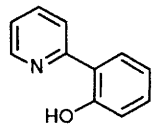

HL^2

Experimental

The NMR spectra were recorded on JEOL GX270 or GX400 spectrometers, electron-impact (EI) mass spectra on a Kratos MS9 instrument, fast-atom bombardment (FAB) mass spectra on a VG-ZAB instrument, UV/VIS spectra on a Perkin Elmer Lambda 2 spectrophotometer and ESR spectra on a Bruker ESP-300E spectrometer. Room-temperature magnetic susceptibility measurements were performed with a Sherwood Scientific MSB-1 balance. Electrochemical experiments were performed using an EG&G PAR model 273A potentiostat. A standard three-electrode configuration was used, with platinum-bead working and auxiliary electrodes and a saturated calomel electrode (SCE) as reference. Ferrocene was added at the end of each experiment as an internal standard; all potentials are quoted *vs.* the ferrocene–ferrocenium couple. The solvent was acetonitrile, purified by distillation from CaH_2. The base electrolyte was 0.1 mol dm^{-3} $[NBu_4][PF_6]$. All solvents were dried by standard methods before use. 2-Bromoanisole and 2-bromopyridine were purchased from Aldrich and used as received. 6-(2-Hydroxyphenyl)-2,2'-bipyridine (HL^1) was prepared as described earlier.[3]

Preparations.—*2-(2-Methoxyphenyl)pyridine.* To an ice-cold mixture of $[Ni(dppe)Cl_2]$ (dppe = $Ph_2PCH_2CH_2PPh_2$) (0.53 g, 1 mmol)[6] and 2-bromopyridine (4.74 g, 30 mmol) in dry tetrahydrofuran (thf, 30 cm^3) under N_2 was added dropwise *via* syringe a solution of the Grignard reagent prepared from 2-bromoanisole (6.74 g, 36 mmol) and magnesium turnings (1.02 g, 42 mmol) in thf (40 cm^3). The mixture was allowed to attain

† *Supplementary data available:* see Instructions for Authors, *J. Chem. Soc., Dalton Trans.*, 1992, Issue 1, pp. xx–xxv.

room temperature and stirred overnight (12 h). The reaction was then quenched by addition of aqueous NH_4Cl, acidified with HCl and the thf removed under reduced pressure. The acidic aqueous solution was washed three times with CH_2Cl_2 (20 cm^3) and then neutralised with aqueous KOH or NH_3. The mixture was then extracted three times with CH_2Cl_2 (20 cm^3), and the combined organic extracts dried ($MgSO_4$) and the solvent removed to give the product as a straw-coloured oil (4.85 g, 87%). It is sufficiently pure for use in the subsequent step, but may be further purified if required by chromatography on silica with CH_2Cl_2–MeOH (98:2) as eluent to give a colourless oil. Mass spectrum (EI): m/z = 185 (M^+) and 154 ($M^+ - CH_3O$). ^{1}H NMR (270 MHz, $CDCl_3$); δ 7.00 (1 H, d, J = 8.3, phenyl H^6), 7.08 (1 H, td, J = 7.5, 1.1, phenyl H^4), 7.19 (1 H, ddd, J = 7.3, 4.9, 1.3, H^5), 7.37 (1 H, td, J = 8.7, 1.8, phenyl H^5), 7.68 (1 H, td, J = 7.7, 1.8, H^4), 7.76 (1 H, dd, J = 7.7, 1.8, phenyl H^3), 7.82 (1 H, d, J = 8.1, H^3) and 8.69 (1 H, ddd, J = 4.9, 1.8, 0.7 Hz, H^6).

2-(2-*Hydroxyphenyl*)*pyridine* (HL^2). This was prepared by demethylation of 2-(2-methoxyphenyl)pyridine (4.8 g) in molten pyridinium chloride (from 16 cm^3 pyridine and 17.6 cm^3 concentrated HCl) under N_2 for 2 h at 190 °C according to a published method.[7] After addition of water to the mixture and neutralisation with aqueous KOH, the crude product was extracted with CH_2Cl_2 (3 × 20 cm^3), dried ($MgSO_4$), and the solvent removed under reduced pressure. The brown oil was purified by chromatography (silica, CH_2Cl_2) to give the product as a yellow oil in 90% yield. Mass spectrum (EI): m/z = 171 (M^+). ^{1}H NMR (270 MHz, $CDCl_3$); δ 6.91 (1 H, td, J = 7.3, 1.1, phenyl H^4), 7.03 (1 H, dd, J = 8.3, 1.1, phenyl H^6), 7.23 (1 H, ddd, J = 6.2, 5.1, 1.1, phenyl H^5), 7.31 (1 H, td, J = 7.1, 1.7, H^5), 7.78–7.87 (2 H, m, H^4 and phenyl H^3), 7.92 (1 H, d, J = 8.4, H^3), 8.50 (1 H, d, J = 5.1 Hz, H^6) and 14.3 (1 H, br s, phenolic OH) (Found: C, 77.7; H, 5.2; N, 8.2. Calc. for $C_{11}H_9NO$: C, 77.2; H, 5.3; N, 8.2%).

The complex $[Ru(bipy)_2L^2][PF_6]$ (bipy = 2,2′-bipyridine) was prepared by reaction of HL^2 (0.084 g, 0.49 mmol) with $[Ru(bipy)_2Cl_2]\cdot 2H_2O$[8] (0.244 g, 0.47 mmol) and triethylamine (0.1 cm^3) in ethanol (25 cm^3) at reflux for 6 h, followed by addition of aqueous KPF_6. The resulting purple precipitate was filtered off, washed with ethanol, dried, and recrystallised from MeCN–Et_2O. Mass spectrum (FAB): m/z = 584 {$[Ru(bipy)_2L^2]^+$, based on ^{102}Ru}. ^{1}H NMR (400 MHz, CD_3CN); δ 6.06 (1 H, dd, J = 8.3, 1.2), 6.46 (1 H, ddd, J = 8.1, 7.0, 1.2), 6.76 (2 H, m), 6.96 (1 H, dt, J = 7.9, 1.2), 7.09 (1 H, ddd, J = 7.3, 5.8, 1.5), 7.14 (2 H, m), 7.36 (1 H, dd, J = 8.1, 1.7), 7.40 (1 H, ddd, J = 5.6, 1.5, 0.7), 7.59 (1 H, ddd, J = 7.6, 5.5, 1.4), 7.71 (2 H, m), 7.78 (3 H, m), 7.88 (1 H, ddd, J = 5.7, 1.4, 0.7), 8.11 (1 H, td, J = 7.9, 1.5), 8.25 (1 H, d, J = 7.8), 8.29 (1 H, d, J = 7.8), 8.46 (1 H, ddd, J = 5.6, 1.5, 0.7), 8.49 (1 H, dt, J = 7.6, 1.1), 8.61 (1 H, dt, J = 8.1, 1.1) and 9.15 (1 H, ddd, J = 5.6, 1.6, 0.9 Hz); for assignments see Fig. 1 (Found: C, 51.1; H, 3.6; N, 9.7. Calc. for $[Ru(bipy)_2L^2][PF_6]$: 51.1; H, 3.3; N, 9.6%).

The complex $[RuL^1_2][PF_6]$ was prepared by reaction of HL^1 (0.15 g, 0.61 mmol) with $RuCl_3\cdot xH_2O$ (0.073 g, *ca.* 0.3 mmol) in ethylene glycol (25 cm^3) at reflux for 2 h followed by cooling and addition of aqueous KPF_6. The resulting dark green precipitate was filtered off, washed with ethanol and dried. The crude material was chromatographed on alumina (Aldrich, activity I) with MeCN–toluene (60:40, v/v) as eluent; the major green fraction was collected and recrystallised from MeCN–Et_2O. Mass spectrum (FAB): m/z = 596 ($[RuL^1_2]^+$, based on ^{102}Ru) (Found: C, 52.5; H, 2.9; N, 9.1. Calc. for $[RuL^1_2][PF_6]\cdot$MeCN: C, 52.2; H, 3.2; N, 9.0%).

Crystal Structure Determinations.—Data were collected using a Siemens R3m/V four-circle diffractometer (293 K, Mo-Kα X-radiation, graphite monochromator, λ = 0.710 73 Å). The data were corrected for Lorentz, polarisation and X-ray absorption effects, the latter by an empirical method based upon azimuthal scan data. The structures were solved by conventional heavy-atom or direct methods and successive Fourier difference syntheses were used to locate all non-hydrogen atoms. All calculations were performed on a DEC micro-Vax II computer with the SHELXTL PLUS system of programs.[9] Scattering factors with corrections for anomalous dispersion were taken from ref. 10. Atom coordinates are listed in Tables 2 and 4.

Additional material available from the Cambridge Crystallographic Data Centre comprises H-atom coordinates, thermal parameters and remaining bond lengths and angles.

$[Ru(bipy)_2L^2][PF_6]\cdot$MeCN. Crystals were grown from MeCN–Et_2O as deep purple prisms and that used had dimensions *ca.* 0.50 × 0.40 × 0.20 mm. Of the 6221 data collected (Wyckoff ω scan, $2\theta \leqslant 50°$), 3790 unique data had $F \geqslant 5\sigma(F)$, and only these were used for structure solution and refinement.

Crystal data. $C_{31}H_{24}F_6N_5OPRu\cdot$MeCN, M = 769.6, monoclinic, space group $P2_1/n$, a = 7.794(4), b = 27.247(12), c = 15.220(9) Å, β = 98.31(4)°, U = 3198(3) $Å^3$, Z = 4, D_c = 1.60 g cm^{-3}, $F(000)$ = 1552, μ(Mo-Kα) = 6.1 cm^{-1}.

All non-hydrogen atoms were refined with anisotropic thermal parameters. Hydrogen atoms were included in calculated positions (C–H 0.96 Å) with fixed isotropic thermal parameters (U_{iso} = 0.08 $Å^2$). Final R = 0.045 (R' = 0.046) with a weighting scheme $w^{-1} = [\sigma^2(F) + 0.0008F^2]$. The final electron-density difference synthesis showed no peaks >0.63 or < −0.47 e $Å^{-3}$.

$[RuL^1_2][PF_6]\cdot$MeCN. Crystals were grown from MeCN–Et_2O as deep green prisms and that used had dimensions *ca.* 0.70 × 0.60 × 0.25 mm. Of the 7732 data collected (Wyckoff ω scan, $2\theta \leqslant 55°$), 6263 unique data had $F \geqslant 4\sigma(F)$, and only these were used for structure solution and refinement.

Crystal data. $C_{32}H_{22}F_6N_4O_2PRu\cdot$MeCN, M = 781.6, triclinic, space group $P\bar{1}$, a = 9.986(3), b = 12.738(3), c = 13.337(4) Å, α = 83.64(2), β = 78.17(2), γ = 74.46°, U = 1597.0(8) $Å^3$, Z = 2, D_c = 1.63 g cm^{-3}, $F(000)$ = 786, μ(Mo-Kα) = 6.2 cm^{-1}.

Non-hydrogen and hydrogen atoms were treated as above. Final R = 0.036 (R' = 0.039) with a weighting scheme $w^{-1} = [\sigma^2(F) + 0.0005F^2]$. The final electron-density difference synthesis showed no peaks >0.43 or < −0.55 e $Å^{-3}$.

Results and Discussion

The mixed pyridine–phenol ligands used in this study were 6-(2-hydroxyphenyl)-2,2′-bipyridine (HL^1), the synthesis and co-ordination chemistry of which we have recently reported,[3–5] and the N,O-bidentate ligand 2-(2-hydroxyphenyl)pyridine (HL^2). Despite the simplicity of HL^2 and its obvious appeal as a ligand (*e.g.* as an analogue of salicylaldimines) it has received very little attention (there is only one report of its use in transition-metal complexes[11]) principally due to the difficulties involved in synthesis of the methylated precursor 2-(2-methoxyphenyl)pyridine. This was originally prepared in 1940 by reaction of pyridine with diazotised *o*-anisidine,[12] but the reaction has the disadvantage that it produces a mixture of 2-, 3- and 4-(2-methoxyphenyl)pyridines which require difficult separation; a recent optimisation of this method gave 2-(2-methoxyphenyl)pyridine in 32% yield.[13] Other preparations are even less satisfactory; reaction of 2-lithioanisole with pyridine produces 2-(2-methoxyphenyl)pyridine in 10% yield,[14] and reaction of pyridine *N*-oxide with anisole in acetic acid gives a yield of 11%,[15] in both cases the crude material requiring considerable purification. It is clear that a proper study of the co-ordination chemistry of HL^2 requires a simpler and more efficient synthesis, and we have developed a straightforward, high-yield preparation of 2-(2-methoxyphenyl)pyridine based on coupling of the Grignard reagent from 2-bromoanisole with 2-bromopyridine in the presence of a nickel catalyst.

The method described here is based on that recently used for the preparation of 3-(4-methoxyphenyl)pyridine in 74% yield,

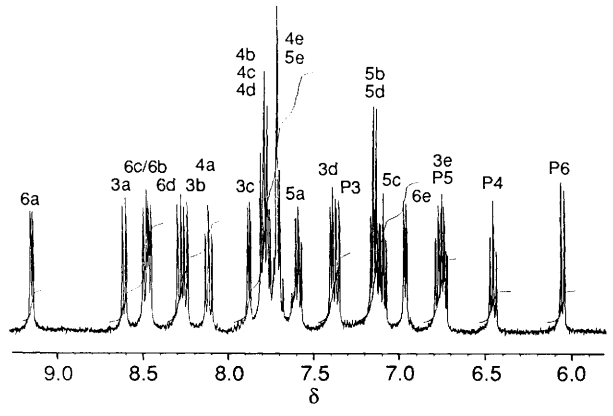

Fig. 1 The ^{1}H NMR spectrum of $[Ru(bipy)_2L^2][PF_6]$ (400 MHz, CD_3CN). Letters a–e refer to pyridyl rings; P denotes the phenyl ring; the numbers are the positions of the protons using the conventional numbering scheme

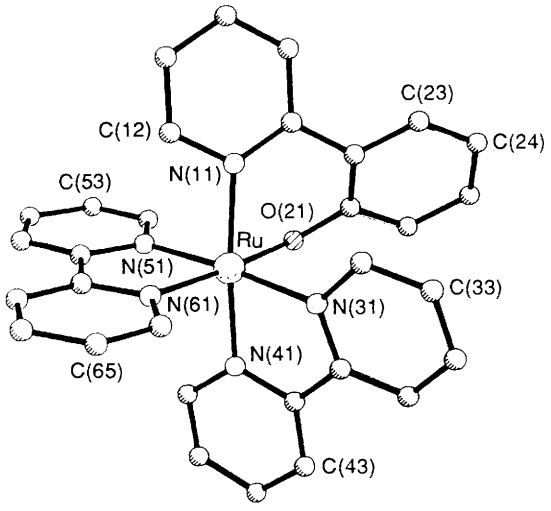

Fig. 2 Structure of the cation of $[Ru(bipy)_2L^2][PF_6]$·MeCN showing the atom numbering scheme

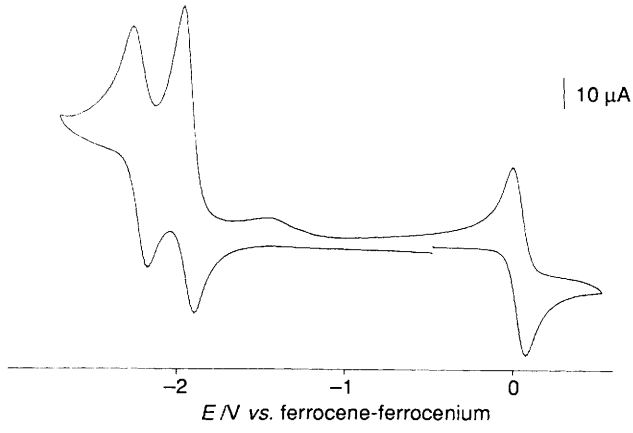

Fig. 3 Cyclic voltammogram of $[Ru(bipy)_2L^2][PF_6]$ in MeCN at 0.5 V s^{-1}

which involved coupling of the Grignard reagent from 4-bromoanisole with 3-bromopyridine using $[Ni(PPh_3)_2Cl_2]$ catalyst.[16] Accordingly we tried the reaction of 2-bromopyridine with the Grignard reagent from 2-bromoanisole with $[Ni(PPh_3)_2Cl_2]$ as catalyst under identical conditions, but the results were disappointing, giving 2-(2-methoxyphenyl)pyridine in only 15% yield. However use of $[Ni(dppe)Cl_2]$ as the coupling catalyst resulted in an 87% yield of virtually pure product; an identical yield was also obtained with $[Ni(dppp)Cl_2]$ as catalyst [dppp = 1,3-bis(diphenylphosphino)propane]. Demethylation with molten pyridinium chloride gave HL^2 in 90% yield, giving an overall yield of 78% for the simple two-step process. The identities of both 2-(2-methoxyphenyl)pyridine and HL^2 were confirmed by mass and ^{1}H NMR spectrometry. Both NMR spectra contain eight resonances in the aromatic region which could be unambiguously assigned by comparison with the spectra of 6-(2-methoxyphenyl)-2,2′-bipyridine and HL^1 respectively. As we have come to expect for ligands of this type, the phenolic proton of HL^2 has a very high chemical shift (δ 14.3) due to intramolecular hydrogen bonding to the adjacent pyridyl N atoms, which forms a six-membered 'chelate' ring.

Reaction of HL^2 with 1 equivalent of $[Ru(bipy)_2Cl_2]$ in ethanol at reflux gave a deep purple solution, from which a purple solid precipitated on addition of KPF_6. Thin-layer chromatography (alumina, MeCN) revealed the complex to be virtually pure. It was recrystallised by diffusion of diethyl ether vapour into a concentrated acetonitrile solution to yield purple plates. The elemental analysis and FAB mass spectrum were, as expected, in accord with the formulation $[Ru(bipy)_2L^2][PF_6]$ in which L^2 acts as a monoanionic bidentate donor. The ^{1}H NMR spectrum of the complex (Fig. 1) shows 24 clearly defined resonances in the aromatic region. With the aid of two-dimensional ^{1}H–^{1}H correlation spectroscopy (COSY) these could be separated into six groups of four, each corresponding to H^3, H^4, H^5 and H^6 of an aromatic ring. The four protons of the phenyl ring can be assigned unambiguously. The resonances of pyridyl ring 'e' are at much lower chemical shift than those of the other pyridyl rings, so ring 'e' is presumably the one *trans* to the electron-donating phenolate. The other sets of protons (a–d) cannot be unambiguously assigned to particular pyridyl rings.

The crystal structure of the cation of $[Ru(bipy)_2L^2][PF_6]$·MeCN is shown in Fig. 2; relevant bond lengths and angles are in Table 1 and atomic coordinates in Table 2. The complex is pseudo-octahedral. The Ru–N bond lengths lie in the range 2.022(4)–2.093(5) Å, which bracket the Ru–N bond length of $[Ru(bipy)_3]^{2+}$ [2.056(6) Å].[17] The longest Ru–N distance in $[Ru(bipy)_2L^2][PF_6]$ is to N(11) (the N atom of L^2) which is probably a steric effect arising from the six-membered chelate ring. The shortest Ru–N distance is to the N atom *trans* to the σ-donating phenolate, which is consistent with improved $Ru(d_\pi)$–bipy(π^*) back bonding due to the increased electron density at the metal centre and with the relative NMR shifts of the protons in this pyridyl ring which indicate an electron-rich environment. The two bipyridines are near-planar (inter-ring torsion angles *ca.* 1 and 4°), whereas L^2 has a torsion angle of *ca.* 34° between the pyridyl and phenolate rings, somewhat larger than the torsion angles of 22–29° observed in $[CoL^2_3]$.[11]

A cyclic voltammogram of $[Ru(bipy)_2L^2][PF_6]$ in acetonitrile is shown in Fig. 3. The Ru^{II}–Ru^{III} couple occurs at $E_{\frac{1}{2}} = +0.03$ V *vs.* the ferrocene–ferrocenium couple and is reversible ($\Delta E_p = 80$ mV at a scan rate of 0.5 V s^{-1} and is virtually independent of scan rate; $i_{pa} \approx i_{pc}$). Under the same conditions the Ru^{II}–Ru^{III} couple of $[Ru(bipy)_2]^{2+}$ occurs at $E_{\frac{1}{2}} = +0.89$ V, so substitution of one π-acidic pyridyl ligand by a σ-donating phenolate ligand results in a decrease of the Ru^{II}–Ru^{III} couple (and hence stabilisation of the higher oxidation state) by 0.86 V. The phenolate group also reduces the charge of the complex cation from +2 to +1 which will result in additional electrostatic stabilisation of the oxidised state. It has been shown that $[Ru(bipy)_3]^{2+}$ has a +3/+4 couple at +2.78 V *vs.* SCE in liquid SO_2 as solvent.[18] It is to be expected that the potential of this redox process (if it is metal-centred) will also decrease in $[Ru(bipy)_2L^2][PF_6]$ and perhaps lie within the solvent window, but no such process was visible; instead there is a totally irreversible ligand-based oxidation at +1.29 V *vs.* ferrocene–ferrocenium (not shown in the figure), which is common to all complexes we have examined which contain phenolate groups as ligands. Finally, reductions occur at −1.93 and −2.19 V *vs.* ferrocene–ferrocenium, which are potentials characteristic of

Table 1 Selected internuclear distances (Å) and angles (°) for $[Ru(bipy)_2L^2][PF_6]$·MeCN

Ru–O(21)	2.064(4)	Ru–N(11)	2.093(5)	Ru–N(31)	2.049(5)	Ru–N(41)	2.046(5)
Ru–N(51)	2.034(5)	Ru–N(61)	2.022(4)	O(21)–C(21)	1.318(6)	N(11)–C(12)	1.351(8)
N(11)–C(16)	1.353(7)	N(31)–C(32)	1.347(7)	N(31)–C(36)	1.349(7)	N(41)–C(42)	1.351(7)
N(41)–C(46)	1.335(7)	N(51)–C(52)	1.343(7)	N(51)–C(56)	1.357(7)	N(61)–C(62)	1.351(8)
N(61)–C(66)	1.346(7)						

O(21)–Ru–N(11)	85.8(2)	O(21)–Ru–N(31)	87.8(2)	N(11)–Ru–N(31)	98.3(2)
O(21)–Ru–N(41)	89.5(2)	N(11)–Ru–N(41)	174.6(2)	N(31)–Ru–N(41)	78.9(2)
O(21)–Ru–N(51)	93.8(2)	N(11)–Ru–N(51)	87.1(2)	N(31)–Ru–N(51)	174.5(2)
N(41)–Ru–N(51)	95.8(2)	O(21)–Ru–N(61)	173.2(2)	N(11)–Ru–N(61)	95.0(2)
N(31)–Ru–N(61)	98.7(2)	N(41)–Ru–N(61)	90.0(2)	N(51)–Ru–N(61)	79.5(2)
Ru–O(21)–C(21)	117.1(3)	Ru–N(11)–C(12)	119.5(4)	Ru–N(11)–C(16)	122.9(4)
C(12)–N(11)–C(16)	117.3(5)	Ru–N(31)–C(32)	126.8(4)	Ru–N(31)–C(36)	115.0(3)
C(32)–N(31)–C(36)	117.8(5)	Ru–N(41)–C(42)	115.3(3)	Ru–N(41)–C(46)	126.7(4)
C(42)–N(41)–C(46)	117.9(5)	Ru–N(51)–C(52)	125.9(4)	Ru–N(51)–C(56)	116.1(4)
C(52)–N(51)–C(56)	117.9(5)	Ru–N(61)–C(62)	115.8(3)	Ru–N(61)–C(66)	126.0(4)
C(62)–N(61)–C(66)	118.1(5)				

Table 2 Atomic positional parameters (fractional coordinates × 10^4) for $[Ru(bipy)_2L^2][PF_6]$·MeCN, with estimated standard deviations (e.s.d.s) in parentheses

Atom	*x*	*y*	*z*	Atom	*x*	*y*	*z*
Ru	861(1)	1127(1)	3043(1)	C(45)	−986(8)	−288(2)	3788(4)
O(21)	2597(5)	1154(1)	4203(2)	C(46)	−171(7)	76(2)	3387(4)
N(11)	2192(6)	1737(2)	2648(3)	N(51)	2434(6)	706(2)	2397(3)
C(12)	2374(8)	1790(2)	1783(4)	C(52)	4026(7)	547(2)	2732(4)
C(13)	3390(9)	2135(3)	1468(4)	C(53)	5012(8)	266(2)	2258(5)
C(14)	4270(9)	2456(3)	2057(5)	C(54)	4362(9)	140(3)	1402(5)
C(15)	4099(8)	2421(2)	2936(5)	C(55)	2745(9)	299(2)	1045(4)
C(16)	3044(7)	2059(2)	3231(4)	C(56)	1788(8)	573(2)	1555(4)
C(21)	2775(6)	1578(2)	4623(3)	N(61)	−656(6)	1040(2)	1859(3)
C(22)	2912(7)	2032(2)	4192(4)	C(62)	28(8)	769(2)	1252(4)
C(23)	3033(8)	2464(2)	4692(5)	C(63)	−867(9)	691(3)	407(4)
C(24)	3083(9)	2460(3)	5589(5)	C(64)	−2483(10)	893(3)	195(5)
C(25)	3041(8)	2010(3)	6019(4)	C(65)	−3201(8)	1158(3)	805(5)
C(26)	2896(7)	1581(2)	5558(4)	C(66)	−2251(7)	1230(2)	1626(4)
N(31)	−868(5)	1492(2)	3702(3)	P	2249(3)	1211(1)	8653(2)
C(32)	−1105(7)	1981(2)	3731(4)	F(1)	915(9)	798(3)	8586(5)
C(33)	−2105(8)	2199(2)	4292(4)	F(2)	3268(10)	943(3)	8024(6)
C(34)	−2906(8)	1912(2)	4847(4)	F(3)	3605(11)	1627(3)	8746(6)
C(35)	−2731(7)	1410(2)	4796(4)	F(4)	1105(12)	1500(3)	9184(6)
C(36)	−1711(6)	1208(2)	4227(3)	F(5)	1373(13)	1457(5)	7853(7)
N(41)	−374(5)	553(2)	3550(3)	F(6)	3117(13)	970(4)	9439(7)
C(42)	−1475(7)	678(2)	4122(4)	C(1)	6610(13)	955(4)	6999(7)
C(43)	−2340(8)	325(2)	4546(4)	C(2)	6852(13)	1383(4)	7543(7)
C(44)	−2078(8)	−163(2)	4375(4)	N	6408(13)	630(4)	6561(6)

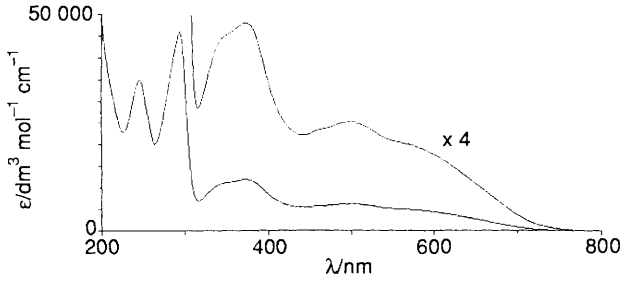

Fig. 4 The UV/VIS spectrum of $[Ru(bipy)_2L^2][PF_6]$ in MeCN

ligand-based processes. The first of these is slightly distorted by an absorption process but the second is fully reversible.

The UV/VIS spectrum of $[Ru(bipy)_2L^2][PF_6]$ is shown in Fig. 4, and may be assigned by comparison with the spectrum of $[Ru(bipy)_3]^{2+}$,[19] taking account of the reduced ligand-field strength of L^2 compared to bipy. First, whereas the lowest-energy ^{1}m.l.c.t. (metal to ligand charge transfer) bands for $[Ru(bipy)_3]^{2+}$ are at 420 and 450 nm, in $[Ru(bipy)_2L^2][PF_6]$ these have moved to 500 and 570 nm and are much broader with a tail out to nearly 800 nm. This is consistent with the decreased ligand-field strength making the $Ru(d_\pi)$ orbitals higher in energy and therefore nearer the ligand π^* orbitals, and inequivalence of the ligands resulting in a range of m.l.c.t. energies. Secondly, the weak metal-centred d–d transition of $[Ru(bipy)_3]^{2+}$ at 340 nm has also moved to lower energy (373 nm) in $[Ru(bipy)_2L^2][PF_6]$ and is much more intense (ε = 12 000 dm^3 mol^{-1} cm^{-1}); this increased intensity is consistent with the lower symmetry, and is also likely to have a contribution from intensity borrowing from other charge-transfer bands. The two intense bands at 294 and 246 nm (ε = 46 000 and 35 000 dm^3 mol^{-1} cm^{-1}) correspond to ligand-centred π–π^* and m.l.c.t. transitions respectively, and are very similar to the analogous absorptions of $[Ru(bipy)_3]^{2+}$. The complex $[Ru(bipy)_2L^2][PF_6]$ does not appear to show luminescence at room temperature.

Reaction of HL^1 with approximately half an equivalent of ruthenium trichloride in ethylene glycol at reflux yielded a dark green solution from which a green solid precipitated on addition of KPF_6, which could be purified by chromatography on alumina with acetonitrile–toluene followed by recrystallisation from acetonitrile–diethyl ether. The FAB mass spectrum, as expected, suggested the formulation $[RuL^1_2][PF_6]$ in which the ruthenium is in oxidation state +3; this was confirmed by

Table 3 Selected internuclear distances (Å) and angles (°) for $[RuL^1{}_2][PF_6]\cdot MeCN$

Ru–N(11)	2.056(2)	Ru–N(21)	2.032(2)	Ru–O(31)	1.965(2)	Ru–N(41)	2.069(3)
Ru–N(51)	2.033(2)	Ru–O(61)	1.947(3)	N(11)–C(12)	1.349(4)	N(11)–C(16)	1.360(4)
N(21)–C(22)	1.358(3)	N(21)–C(26)	1.367(4)	O(21)–C(31)	1.340(4)	N(41)–C(42)	1.345(4)
N(41)–C(46)	1.356(4)	C(46)–C(52)	1.479(4)	N(51)–C(52)	1.357(4)	N(51)–C(56)	1.359(3)
O(61)–C(61)	1.330(3)						

N(11)–Ru–N(21)	79.7(1)	N(11)–Ru–O(31)	170.9(1)	N(21)–Ru–O(31)	93.6(1)
N(11)–Ru–N(41)	85.2(1)	N(21)–Ru–N(41)	99.4(1)	O(31)–Ru–N(41)	89.9(1)
N(11)–Ru–N(51)	98.4(1)	N(21)–Ru–N(51)	177.9(1)	O(31)–Ru–N(51)	88.2(1)
N(41)–Ru–N(51)	79.6(1)	N(11)–Ru–O(61)	89.9(1)	N(21)–Ru–O(61)	86.3(1)
O(31)–Ru–O(61)	95.8(1)	N(41)–Ru–O(61)	171.7(1)	N(51)–Ru–O(61)	94.6(1)
Ru–N(11)–C(12)	126.8(2)	Ru–N(11)–C(16)	114.1(2)	C(12)–N(11)–C(16)	118.8(2)
Ru–N(21)–C(22)	115.2(2)	Ru–N(21)–C(26)	124.1(2)	C(22)–N(21)–C(26)	120.6(2)
Ru–O(31)–C(31)	122.5(2)	Ru–N(41)–C(42)	126.6(2)	Ru–N(41)–C(46)	114.9(2)
C(42)–N(41)–C(46)	118.5(3)	Ru–N(51)–C(52)	115.4(2)	Ru–N(51)–C(56)	123.9(2)
C(52)–N(51)–C(56)	120.6(2)	Ru–O(61)–C(61)	123.9(2)		

Table 4 Atomic positional parameters (fractional coordinates × 10^4) for $[RuL^1{}_2][PF_6]\cdot MeCN$, with e.s.d.s in parentheses

Atom	*x*	*y*	*z*	Atom	*x*	*y*	*z*
Ru	131(1)	1828(1)	2002(1)	C(46)	−1485(3)	677(2)	1139(2)
N(11)	−1253(3)	1852(2)	3376(2)	N(51)	657(2)	195(2)	1823(2)
C(12)	−1567(4)	981(3)	3955(2)	C(52)	−278(3)	−173(2)	1437(2)
C(13)	−2605(5)	1090(3)	4812(3)	C(53)	−125(4)	−1270(2)	1363(3)
C(14)	−3373(5)	2121(4)	5088(3)	C(54)	978(4)	−2005(3)	1729(3)
C(15)	−3062(4)	3023(3)	4505(3)	C(55)	1938(4)	−1637(2)	2110(3)
C(16)	−1986(3)	2871(3)	3661(2)	C(56)	1821(3)	−513(2)	2104(2)
N(21)	−460(2)	3455(2)	2214(2)	O(61)	1654(2)	1764(2)	2732(2)
C(22)	−1523(3)	3769(2)	3020(2)	C(61)	2801(3)	937(2)	2706(2)
C(23)	−2072(4)	4853(3)	3234(3)	C(62)	2936(3)	−122(2)	2407(2)
C(24)	−1545(4)	5626(2)	2595(3)	C(63)	4271(3)	−882(3)	2419(3)
C(25)	−459(4)	5311(2)	1793(3)	C(64)	5357(4)	−637(3)	2739(3)
C(26)	142(3)	4206(2)	1607(2)	C(65)	5177(4)	393(3)	3059(3)
O(31)	1231(2)	2007(1)	621(1)	C(66)	3940(3)	1170(3)	3040(3)
C(31)	1828(3)	2845(2)	334(2)	P	6392(1)	4920(1)	6920(1)
C(32)	1377(3)	3863(2)	792(2)	F(1)	7825(3)	4129(3)	6450(3)
C(33)	2206(3)	4619(2)	416(3)	F(2)	6283(4)	5458(3)	5810(2)
C(34)	3332(4)	4423(3)	−380(3)	F(3)	7182(4)	5748(3)	7127(2)
C(35)	3703(3)	3448(3)	−854(3)	F(4)	6527(3)	4323(2)	8026(2)
C(36)	2964(3)	2670(2)	−487(2)	F(5)	5597(3)	4046(3)	6738(2)
N(41)	−1535(3)	1702(2)	1361(2)	F(6)	4924(3)	5661(3)	7393(2)
C(42)	−2641(4)	2520(3)	1170(3)	C(1)	1297(6)	2364(4)	5514(4)
C(43)	−3699(4)	2353(3)	753(3)	C(2)	869(5)	3310(4)	4887(4)
C(44)	−3622(4)	1321(3)	479(3)	N	1611(9)	1619(5)	6015(6)
C(45)	−2494(3)	470(3)	673(3)				

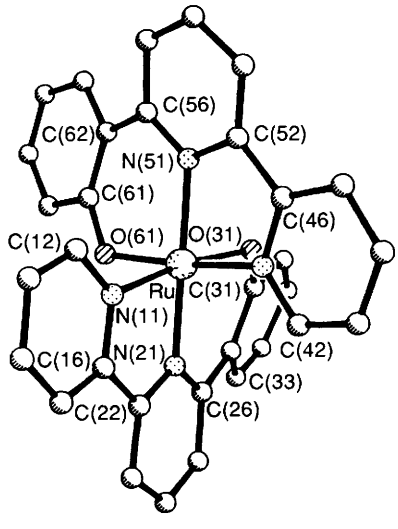

Fig. 5 Structure of the cation of $[RuL^1{}_2][PF_6]\cdot MeCN$ showing the atom numbering scheme

elemental analysis of single crystals which also indicated the presence of one molecule of acetonitrile in the crystal per complex molecule.

The crystal structure of $[RuL^1{}_2][PF_6]\cdot MeCN$ has been determined. The structure of the complex cation is shown in Fig. 5; relevant bond lengths and angles are in Table 3 and atomic coordinates in Table 4. Again the structure is pseudo-octahedral, with each independent terdentate ligand being deprotonated and binding meridionally. The ligand conformations are similar to those observed in $[Cu_2L^1{}_2(\mu\text{-}MeCO_2)][PF_6]$ and $[CoL^1{}_2][PF_6]$,[3] with small torsion angles between the two pyridyl rings (*ca.* 3 and 5°) and larger ones between the central pyridyl and terminal phenolate rings (*ca.* 20 and 18° respectively). The bite angles between the terminal N and O donor atoms of each independent ligand are 170.9 and 171.7°. The Ru–N distances lie within the range 2.032(2)–2.069(3) Å, *i.e.* within the same range as for $[Ru(bipy)_2L^2][PF_6]_2$. This perhaps surprising similarity of the ruthenium–pyridyl bond lengths in both ruthenium(II) and ruthenium(III) complexes has been noted before, and it was suggested that the expected shortening of the bonds [due to contraction of the ruthenium(III) centre compared to Ru^{II}, and a higher

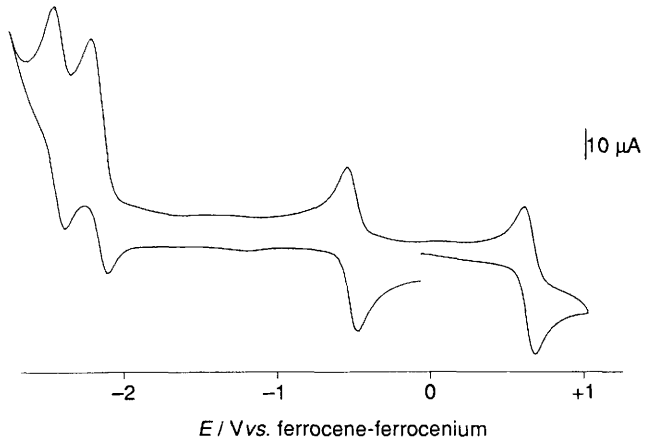

Fig. 6 Cyclic voltammogram of $[RuL^1{}_2][PF_6]$ in MeCN at 0.5 V s^{-1}

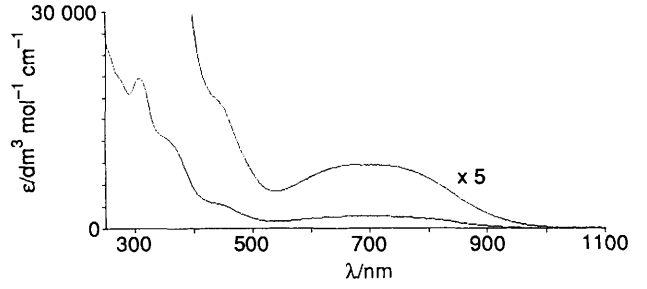

Fig. 7 The UV/VIS spectrum of $[RuL^1{}_2][PF_6]$ in MeCN

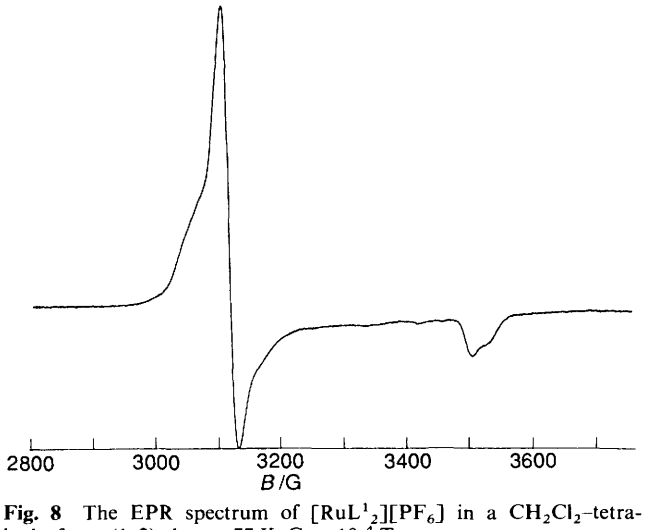

Fig. 8 The EPR spectrum of $[RuL^1{}_2][PF_6]$ in a CH_2Cl_2–tetrahydrofuran (1:2) glass at 77 K; G = 10^{-4} T

electrostatic component to the Ru–N interaction] is cancelled by the reduction in $Ru(d_\pi)$–bipy(π^*) back bonding (due to decreased occupation and lower energy of the 't_{2g}' orbital set).[20] In contrast the ruthenium–phenolate bond lengths, where back bonding is not operative, have dropped from 2.064(4) Å in $[Ru(bipy)_2L^2][PF_6]_2$ to 1.965(2) and 1.947(3) Å in $[RuL^1{}_2][PF_6]$. Owing to the decrease in $Ru(d_\pi)$–bipy(π^*) back bonding it is no longer the case that the shortest Ru–N bonds are those *trans* to the Ru–O bonds.

A cyclic voltammogram of $[RuL^1{}_2][PF_6]$ in acetonitrile is shown in Fig. 6. There are four reversible waves visible within the solvent window. The Ru^{II}–Ru^{III} couple is at −0.51 V *vs.* ferrocene–ferrocenium; compared to $[Ru(bipy)_2L^2][PF_6]$ it had dropped by 0.57 V due to the presence of the second phenolate residue in the co-ordination sphere, so that the metal centre is now in the +3 oxidation state and the Ru^{II}–Ru^{III} couple is a reduction. This further decrease in the metal-based redox-potentials now brings the Ru^{III}–Ru^{IV} couple into the solvent window, at +0.65 V *vs.* ferrocene–ferrocenium. The +4 oxidation state for ruthenium is normally associated with halide or oxide ligands, the latter complexes having potential as organic oxidants;[21] this complex is therefore rather unusual in allowing access to the +4 state with π-acidic ligands in the co-ordination sphere. There are also two reductions, at $E_{\frac{1}{2}}$ = −2.15 and −2.44 V *vs.* ferrocene–ferrocenium, which are in the region typical of ligand-based processes. Finally, there is a totally irreversible (probably ligand-based) oxidation at +1.53 V (not shown in the figure).

The UV/VIS spectrum of $[RuL^1{}_2][PF_6]$ is shown in Fig. 7, and may be partially assigned by comparison with the spectrum of $[Ru(bipy)_3]^{3+}$,[22] The broad, relatively weak absorption centred at 680 nm, which is responsible for the intense green colour of the complex, is probably a π(bipy)–t_{2g}(Ru) ligand-to-metal charge transfer (l.m.c.t.) process, since its position is very similar to that of the l.m.c.t. absorption of $[Ru(bipy)_3]^{3+}$ (676 nm), although it is much more intense (ε = 1900 as opposed to 409 dm^3 mol^{-1} cm^{-1}). The possibility that it arises from phenolate to Ru^{III} l.m.c.t. cannot be excluded however. The unusually low intensity of the l.m.c.t. band of $[Ru(bipy)_3]^{3+}$ has been remarked upon,[22,23] and it has been suggested that it is due to coupling of the l.m.c.t. process with a formally disallowed ligand–field d–d transition.[23] Although this seems unlikely since the low energy of the transition is inconsistent with the large ligand-field splitting expected for $[Ru(bipy)_3]^{3+}$, it does explain why the band becomes much more intense in $[RuL^1{}_2][PF_6]$ since the lower symmetry (approximately C_{2v} at the metal centre) would enhance any d–d character of the transition. The intense band at 307 nm (ε = 22 000 dm^3 mol^{-1} cm^{-1}) is a ligand-centred π–π* transition. There are also shoulders at 360 and 440 nm whose nature is uncertain.

The EPR spectrum of $[RuL^1{}_2][PF_6]$ as a frozen glass at 77 K is shown in Fig. 8. It comprises an intense signal at g = 2.16 and a much weaker one at g = 1.92. These are similar in appearance (although not in position) to the signals of $[Ru(bipy)_3]^{3+}$.[24]

To complete this series of compounds we tried to prepare the complex $[RuL^2{}_3]$, with a $(pyridine)_3(phenolate)_3$ donor set, in the expectation that it would show a facile Ru^{III}–Ru^{IV} oxidation. Reaction of $RuCl_3$ with 3 equivalents of HL^2 in ethylene glycol at reflux quickly produced a deep blue solution which slowly (over about 4 h) became deep green. However a TLC analysis of the mixture showed numerous overlapping coloured spots (blue, green and brown) which could not easily be separated. Varying the reaction time and conditions produced equally intractable mixtures with varying ratios of the different components. We did succeed, after extensive chromatography, in isolating a few milligrams of a green material whose FAB mass spectrum showed a peak (amongst others) at the mass appropriate for $[RuL^2{}_3]$, but the elemental analysis was unsatisfactory. Further attempts to prepare and isolate $[RuL^2{}_3]$ are in progress.

Acknowledgements

We thank Drs. Martin Hayes and Martin Murray for recording the NMR spectra and John Maher for the EPR spectrum, the SERC mass spectrometry facility at Swansea for the FAB mass spectra, Dr. Ken MacNeil for the EI mass spectra, and the Nuffield Foundation for financial support. We thank the SERC for a grant to purchase the EPR spectrometer.

References

1 E. C. Constable, *Adv. Inorg. Chem. Radiochem.*, 1986, **30**, 69.
2 E. C. Constable, *Adv. Inorg. Chem. Radiochem.*, 1989, **34**, 1.
3 J. C. Jeffery, E. Schatz and M. D. Ward, *J. Chem. Soc., Dalton Trans.*, 1992, 1921.
4 J. C. Jeffery and M. D. Ward, *J. Chem. Soc., Dalton Trans.*, 1992, 2119.
5 B. M. Holligan, J. C. Jeffery and M. D. Ward, previous paper.
6 G. R. Van Hecke and W. D. Horrocks, *Inorg. Chem.*, 1966, **5**, 1968.

7 C. O. Dietrich-Buchecker and J.-P. Sauvage, *Tetrahedron*, 1990, **46**, 503.
8 B. P. Sullivan, D. J. Salmon and T. J. Meyer, *Inorg. Chem.*, 1978, **17**, 3334.
9 G. M. Sheldrick, SHELXTL program for use with a Siemens X-Ray system, Cambridge, 1976, updated Göttingen, 1981.
10 *International Tables for X-Ray Crystallography*, Kynoch Press, Birmingham, 1974, vol. 4.
11 P. Ganis, A. Saporito, A. Vitagliano and G. Valle, *Inorg. Chim. Acta*, 1988, **142**, 75.
12 J. W. Haworth, I. M. Heilbron and D. H. Hey, *J. Chem. Soc.*, 1940, 358.
13 G. Riggio, W. H. Hopff, A. A. Hofmann and P. G. Waser, *Helv. Chim. Acta*, 1983, **66**, 1039.
14 T. A. Geisman, M. J. Schlatter, I. D. Webb and J. D. Roberts, *J. Org. Chem.*, 1946, **11**, 741.
15 T. Cohen and G. L. Deets, *J. Org. Chem.*, 1972, **37**, 55.
16 J.-P. Sauvage and M. D. Ward, *Inorg. Chem.*, 1991, **30**, 3869.
17 D. P. Rillema, D. S. Jones and H. A. Levy, *J. Chem. Soc., Chem. Commun.*, 1979, 849.
18 J. G. Gaudiello, P. R. Sharp and A. J. Bard, *J. Am. Chem. Soc.*, 1982, **104**, 6373; J. G. Gaudiello, P. G. Bradley, K. A. Norton, W. H. Woodruff and A. J. Bard, *Inorg. Chem.*, 1984, **23**, 3.
19 A. Juris, V. Balzani, F. Barigelletti, S. Campagna, P. Belser and A. von Zelewsky, *Coord. Chem. Rev.*, 1988, **84**, 85.
20 D. W. Pehlps, E. M. Kahn and D. J. Hodgson, *Inorg. Chem.*, 1975, **14**, 2486.
21 C.-M. Che, W.-H. Leung, C.-K. Li and C.-K. Poon, *J. Chem. Soc., Dalton Trans.*, 1991, 379; C.-M. Che, C. Ho and T.-C. Lau, *J. Chem. Soc., Dalton Trans.*, 1991, 1901; N. Grover and H. H. Thorp, *J. Am. Chem. Soc.*, 1991, **113**, 7030; W. P. Griffith, *Transition Met. Chem.*, 1991, **15**, 251; M. S. Thompson and T. J. Meyer, *J. Am. Chem. Soc.*, 1982, **104**, 5070; L. Roecker and T. J. Meyer, *J. Am. Chem. Soc.*, 1987, **109**, 746.
22 G. M. Bryant and J. E. Ferguson, *Aust. J. Chem.*, 1971, **24**, 275.
23 R. J. P. Williams, *J. Am. Chem. Soc.*, 1953, **75**, 2163.
24 R. E. DeSimone and R. S. Drago, *J. Am. Chem. Soc.*, 1970, **92**, 2343.

Received 26*th June* 1992; *Paper* 2/03385B